Nanoscale

PAPER

View Article Online
View Journal | View Issue

Cite this: *Nanoscale*, 2022, **14**, 6220

Post-exfoliation functionalisation of metal–organic framework nanosheets *via* click chemistry†

Joshua Nicks and Jonathan A. Foster *

The liquid exfoliation of layered metal–organic frameworks (MOFs) to form nanosheets (MONs) exposes buried functional groups making them useful in a range of sensing and catalytic applications. Here we show how high yielding click reactions can be used post-exfoliation to systematically modify the surface chemistry of MONs allowing for tuning of their surface properties and their use in new applications. A layered amino-functionalised framework is converted through conventional post-synthetic functionalisation of the bulk MOF to form azide functionalised frameworks of up to >99% yield. Ultrasonic liquid exfoliation is then used to form few-layer nanosheets, which are further functionalised through post exfoliation functionalisation using Cu(I)-catalysed azide–alkyne cycloaddition reactions. Here we demonstrate the advantages of post-exfoliation functionalisation in enabling: (1) a range of functional groups to be incorporated in high yields; (2) tuning of nanosheet surface properties without the need for extensive recharacterisation; (3) the addition of fluorescent functional groups to enable their use in the sensing of hazardous nitrobenzene. We anticipate that the versatility of different functional groups that can be introduced through high yielding click reactions will lead to advances in the use of MONs and other 2D materials for a variety of applications.

Received 18th January 2022,
Accepted 3rd April 2022

DOI: 10.1039/d2nr00346e

rsc.li/nanoscale

Introduction

The exfoliation of layered materials to form two-dimensional nanosheets results in a dramatic increase in their surface area and exposes functional groups that would otherwise be buried within the bulk material.[1] Ultrasound assisted liquid exfoliation is a simple and scalable approach that has been extensively applied to a wide range of two-dimensional materials including graphene,[2] hexagonal boron nitride,[3] and transition metal dichalcogenides.[4,5] However, the surfaces of most of these simple inorganic nanosheets can be difficult to modify without impacting the unique properties that arise from their reduced dimensionality. For example, oxidation of hydrophobic graphene introduces a range of different functional groups at random positions (*e.g.* hydroxyl, aldehyde, carboxylic acid groups) enabling it to be dispersed readily in water, but at the cost of degrading it's electronic and mechanical properties.[6] Non-covalent approaches have been developed which avoid introducing defects, but the functional groups are only relatively weakly attached and at poorly defined positions.[7]

One potential solution to these issues is the use of molecular 2D materials formed from molecular building blocks such as covalent-organic (CONs),[8,9] hydrogen-bonded organic (HONs),[10] and most prolifically metal–organic nanosheets (MONs).[11–13] These materials have a modular structure which allows different functional groups to be introduced easily without changing the underlying structure. Their crystalline nature also mean functional groups are presented on the surface in a well-defined, periodic way in contrast to the functional groups of most 2D materials.[14–16] This tunability and predictability makes MONs ideal for a diverse range of sensing, catalysis, electronic and separation applications.[17] However, the scope of these pre-synthetic approaches to modification are limited in terms of the size and functionality of groups that can be introduced, as they must not impede or interfere with the formation of the supramolecular structure.[18] Each modification also affects the strength of inter layer interactions changing the particle size distribution and sometimes structure of the exfoliated material requiring extensive characterisation and optimisation for each new nanosheet.

Covalent post-synthetic functionalisation (PSF) is a widely used approach for introducing new functional groups incompatible with synthesis conditions to metal–organic frameworks

Department of Chemistry, University of Sheffield, Sheffield, UK.
E-mail: jona.foster@sheffield.ac.uk

†Electronic supplementary information (ESI) available: Full experimental details, synthetic procedures and exfoliation studies. See DOI: https://doi.org/10.1039/d2nr00346e

(MOFs).[18,19] PSF of MOFs is inherently limited by the pore size, with large functional groups not able to diffuse through small pore sites and reacted groups blocking further functionalisation. This is not a problem for MONs, as reactive groups are instead presented on the surface, potentially allowing for a much more diverse range of functionalisation options. Beyond our own work, to our knowledge there is only one other example of the covalent PSF of a MON system which is by Lin *et al.* in which amino-benzenetribenzoate ligands in a Zr_6-based MON are functionalised with two thiocyanate-tagged dyes to enable ratiometric sensing of glutathione and pH.[20] Other forms of PSF such as coordinative modification of SBU's or post-synthetic metalation have also been exploited in these Zr_6-type MONs. For example, elegant work by Lan and Lin *et al.* shows how capping groups of Hf_{12} clusters can be exchanged with triflate groups for tandem Lewis acidic and photoredox catalysis,[21] and catalytically active metal ions can be added to co-ordinating ligand sites in order to facilitate multistep catalytic and photocatalytic reactions.[22,23]

In our previous work we have used liquid exfoliation to obtain a wide range of paddlewheel-based (PW) MOFs which we have used in sensing, catalysis and solar cell applications.[24–26] We recently demonstrated that reaction of 1,3-propansultone with a layered amino-functionalised Cu-PW MOF can simultaneously aid exfoliation into thinner nanosheets and introduce new functionalities for catalysis. PSF occurred on the bulk MOF and the degree of functionalisation was limited to 25% which indicated the size of the polysulfonate groups meant that there was only space for one of the four amine linkers surrounding each pore to be functionalised.[27] In this case, we took advantage of the mixed functionalities on the surface to facilitate a two-step, one-pot tandem reaction. However, coverage and the size of functional groups that can be introduced using this approach is inherently limited by pore size which is detrimental to many applications. This motivated us to develop versatile and high yielding chemistry that would enable us to offer a toolkit to systematically functionalise the surface of the MONs with a diverse range of groups and higher coverage.

In this work, we use click chemistry to undertake post-exfoliation functionalisation in order to modify the surface properties of MONs and impart new functionality. Post-exfoliation functionalisation of nanosheets has the advantage over functionalising bulk frameworks of removing the steric constraints of introducing functionalities within the pores of a MOF. It also allows the exfoliation of a single framework to be optimised and characterised, but then it's surface properties systematically changed and new functionalities introduced. Specifically, we employ Cu(I) catalysed azide–alkyne cycloaddition click chemistry, chosen due to the regioselectivity, versatility, high yield of the reaction under mild conditions, and the lack of side products, such as acids or water, that could impair the coordination bonds of the framework.[28] We show that the surface properties of these materials can be programmed using this technique by adding photo-functional groups to the nanosheets enabling them to sense nitrobenzene.

Results and discussion

Synthesis of Cu(N_3-BDC)(DMF) MOF *via* PSF

A layered amino-MOF, Cu(NH_2-BDC)(DMF), was prepared according to our previously published solvothermal method.[29] Cu(NH_2-BDC)(DMF) was then post-synthetically functionalised by treatment with *t*-butyl nitrite (*t*-BuONO) and up to 10.5 equivalents of azido-trimethylsilane (TMS-N_3) in THF to obtain Cu(N_3-BDC)(DMF) shown in Fig. 1a. This is a common route to azide-functionalised coordination polymers, which utilises more mild conditions than typical diazonium salt conversions.[30–32]

^{1}H NMR spectroscopy of the digested MOF samples confirmed the conversion of the amino- into the azido-terephthalate linker. These spectra are identical to the spectrum obtained for the free linker prepared form 2-aminoterephthalic acid (Fig. S1†) and other literature reports which have utilised this PSF method.[33] FT-IR spectroscopy and mass spectrometry further confirmed PSF had occurred. A comparison between the FT-IR spectra of the amino- and azido-MOFs clearly showed the formation of the asymmetric ν(N═N═N) stretch at 2100 cm^{-1} and the loss of the two ν(N–H) stretching bands in the 3500–3350 cm^{-1} region (Fig. S6†). Mass spectrometry of the digested azido-MOF also indicates the presence of the functionalised linker, $[M]^-$ = 206.0, as well as its distinctive fragmentation pattern, shown in Fig. S7.† Furthermore, NMR studies show the degree of functionalisation could be controlled in a linear fashion by varying the number of equivalents of TMS-N_3 added, as shown in Fig. 1b–d.

X-ray powder diffraction studies (Fig. 1c) of the 100% converted sample show a new pattern. This is to be expected, as the parent amino-framework consists of densely packed layers, and it clear that full conversion to azides cannot proceed without a change in unit cell parameters. Pawley refinement of the 100% functionalised pattern confirmed increases in each lattice parameter and the unit cell volume (Fig. S8 and Table S2†). Remnants of the amino phase are seen in patterns with 20–52% functionalisation but the dominance of the azido-pattern indicates that functionalisation, and thus expansion, is taking place relatively uniformly throughout the sample. Interestingly, our previous studies functionalising Cu(NH_2-BDC) with 1,3-propansultone resulted in no change in unit-cell dimensions however the degree of functionalisation was limited to 25%. We attributed this to the functional group occupying pore space but in this case 100% functionalisation was achieved with a corresponding increase in unit cell parameters.

SEM images of both the amino- and azido-MOFs provided confirmation that there were no significant changes in crystallite size or morphology observed following conversion (Fig. S9†), with both samples forming aggregates <1–15 μm in size.

Attempts to incorporate the azide linker pre-synthetically were unsuccessful. Under identical solvothermal conditions to the Cu(NH_2-BDC)(DMF) synthesis, which is performed at 100 °C, a black solid was obtained, which we attribute to thermal decomposition of the azide moiety. When performed

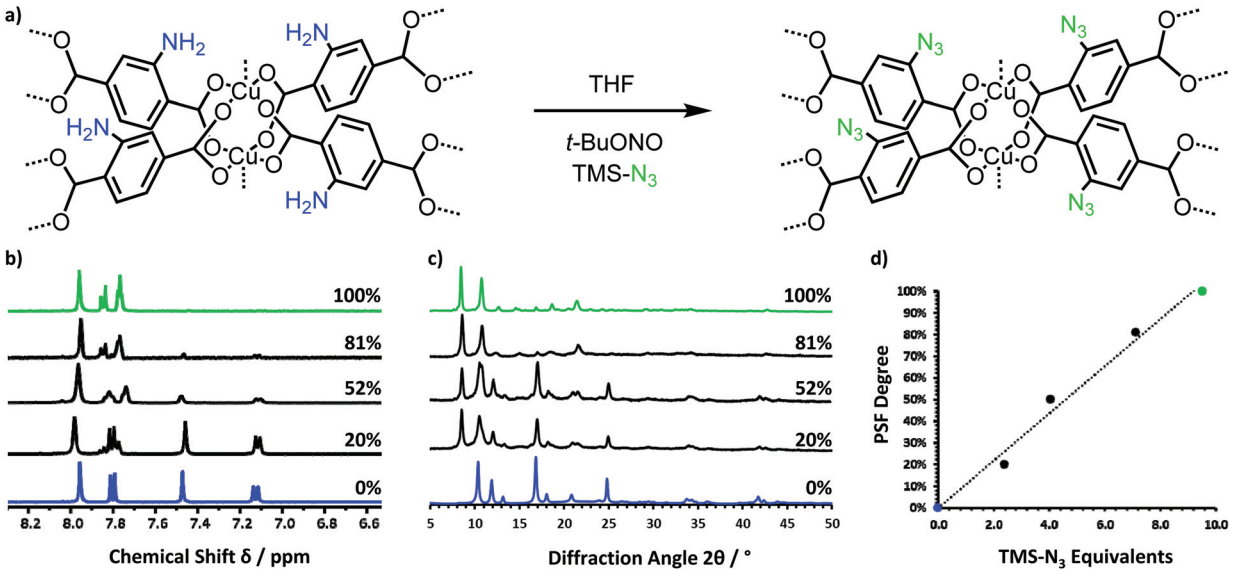

Fig. 1 (a) Scheme showing the post-synthetic functionalisation of the amino-functionalised layered MOF, Cu(NH_2-BDC)(DMF), into the azido-functionalised MOF, Cu(N_3-BDC)(DMF). (b) Stack plot of ^{1}H NMR spectra showing the increasing degree of PSF with increasing equivalents of TMS-N_3 added, with Cu(NH_2-BDC)(DMF) shown in blue, mixed ligand MOFs in black and Cu(N_3-BDC)(DMF) in green. (c) Stack plot of XRD patterns showing the phase change between the fully amino-functionalised MOF (blue) and the fully azido-functionalised MOF (green). (d) Plot showing the tunable degree of conversion from the amino-MOF to the azido-MOF by altering the equivalents of TMS-N_3 used. Higher zoom figures are shown in Fig. S3–5.†

at room temperature, similar amorphous black solids were formed.

This post-synthetic route therefore not only gives access to the azido-functionalised MOF, it also grants the ability to control the amine–azide ratio on the MOF surfaces, allowing for unique control over the surface functionalities of the resulting nanosheets obtained from exfoliation. As this study focuses on post-exfoliation functionalisation *via* click chemistry, all further experiments were performed using ≥99% azido-functionalised samples.

Exfoliation of Cu(N_3-BDC)(DMF) into MONs

Exfoliation of the layered azido-MOF was performed using a previously reported setup (shown in Fig. S10†) designed to regulate temperature and minimise hot-spots.[25] Cu(N_3-BDC)(DMF) was suspended in acetonitrile, and sonicated at 80 kHz for 12 hours, followed by centrifugation for 1 hour at 362*g* (1500 rpm) to remove unexfoliated material and larger fragments.

Suspensions of both the amino- and azido-MON systems exhibit strong Tyndall scattering indicating the presence of nanomaterial in colloidal suspension (Fig. 2e). AFM imaging shows the azido-analogue exfoliates into thinner nanosheets than those of the amino-MOF (Fig. 2a and b, and S11†). Size distribution analysis gives an average thickness of 25 ± 19 nm for the amino-nanosheets, and a significantly thinner 8 ± 7 nm thickness for the azido-MONs (Fig. 2c and d, S12 and S13†). Analysis of the aspect ratios (the ratio between a nanosheets thickness and its largest lateral dimension) also suggests that the azido MONs are much more "sheet"-like, with an average aspect ratio of 20 ± 10, significantly higher than the 10 ± 4.5 value observed for the unfunctionalised sheets. It is also noteworthy that the azido nanosheets are significantly less angular, something we have observed previously with few-layer nanosheets, suggesting that a reduction in thickness can also lead to increased fragmentation during exfoliation.[10,29]

The size distribution analysis also indicates a reduction in the lateral size of the nanosheets obtained upon azidification, with the amino-MONs demonstrating an average largest lateral size of 175 ± 48 nm, with 100 ± 33 nm for the azido MONs. This trend is further supported by dynamic light scattering particle sizing, which indicates a smaller average size for the azido-MONs, with a narrower size distribution, shown in Fig. S14.† It should be noted that the average lateral sizes given by DLS are smaller than those obtained from AFM analysis, consistent with previous reports that implicate the assumption of spherical particles reduces the obtained sizes.[34]

Nanosheets suspensions had strong colloidal stability, with no aggregation-induced precipitation observed after two weeks. The concentrations of the nanosheet suspensions were determined by absorption spectroscopy, which indicated concentrations of 0.4 and 0.5 mg mL^{-1} for the amino- and azido-nanosheets respectively (Fig. S15–17†), which is further corroborated by mass yields of the dried suspensions (~2.3 mg and 2.9 mg respectively). Zeta potential measurements of the two suspensions indicated values of −23.0 and −35.8 mV for Cu(NH_2-BDC) and Cu(N_3-BDC) nanosheets respectively, indicating stronger colloidal stability and more favourable nanosheet–solvent interactions for the Cu(N_3-BDC) MON suspension in acetonitrile.

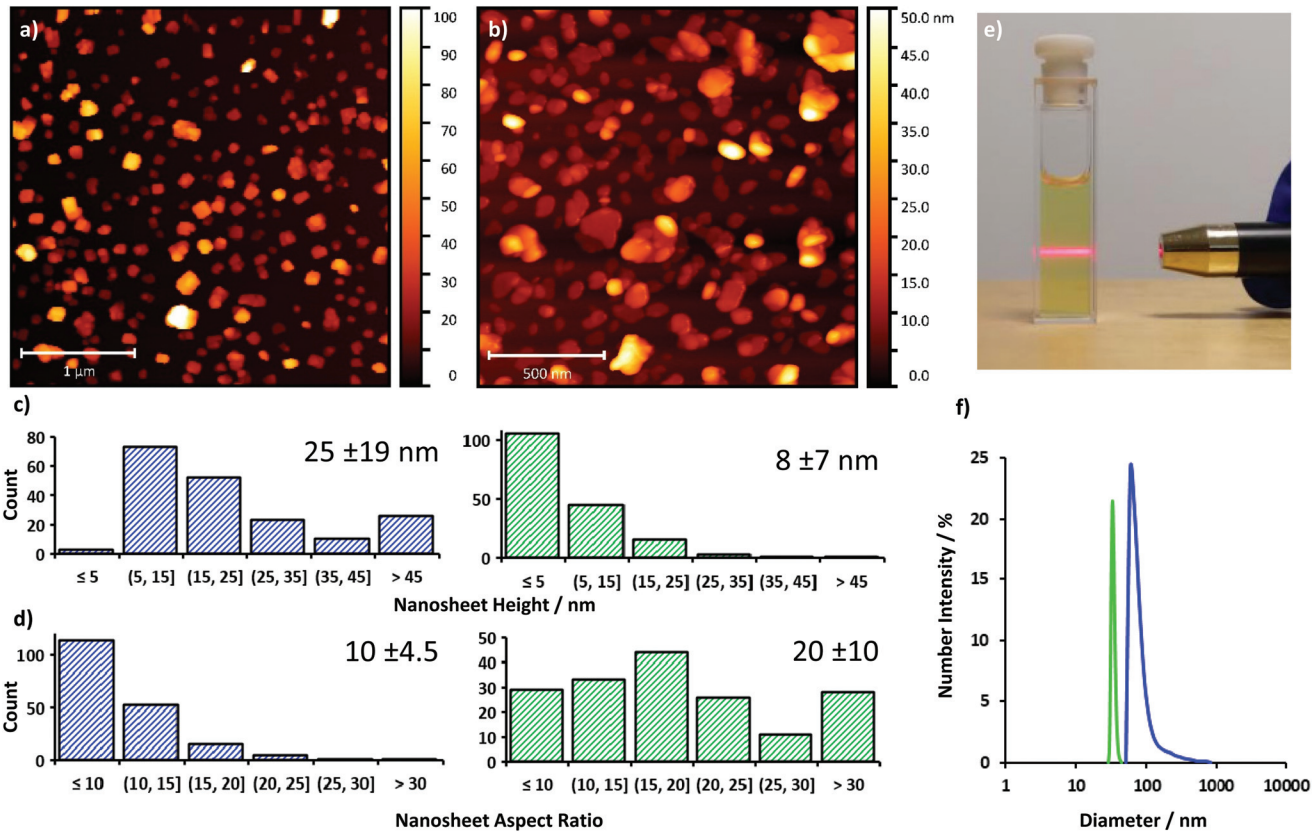

Fig. 2 AFM topographical images of (a) Cu(NH_2-BDC) and (b) Cu(N_3-BDC) nanosheets exfoliated in acetonitrile. (c) Nanosheet thickness histograms for Cu(NH_2-BDC) (blue) and Cu(N_3-BDC)(DMF) nanosheets (green), with inset values for average thickness and standard deviation. (d) Nanosheet aspect ratio histograms for Cu(NH_2-BDC) (blue) and Cu(N_3-BDC) nanosheets (green), with inset values for average aspect ratio and standard deviation. (e) Tyndall scattering images of Cu(N_3-BDC) nanosheets. (f) Particle size distribution data obtained from DLS for Cu(NH_2-BDC) nanosheets (blue) and Cu(N_3-BDC) nanosheets (green).

In order to confirm the phase purity of the material had been maintained post-exfoliation, XRD analysis of the nanosheets was performed after removal of the solvent by evaporation. Peaks in the diffraction pattern of the MONs are observed to be much broader and some reflections are absent (Fig. S18†). This is attributed to the reduction in long-range order associated with exfoliation of the layered framework, reflected in the crystallite domain sizes calculated *via* Scherrer analysis, of 32.2 nm and 17.4 nm for the layered and exfoliated systems respectively. ^{1}H NMR spectroscopy of the digested nanosheets (Fig. S19†) indicates a loss of the coordinated DMF solvent, which is consistent with our previous results for PW-based MOFs exfoliated in acetonitrile.[29,35] It's also worth highlighting that as previously noted, the bulky azide groups result in an expanded inter-layer distance which may also contribute to the enhanced exfoliation observed by AFM.

Overall, the azide functionalised MONs form significantly thinner nanosheets with higher colloidal stabilities which is attributed to increased surface charge and an expansion in inter-layer distance compared to the amino-MONs. These nanosheets are therefore ideal candidates for exploring post-exfoliation functionalisation, as the majority of their azide groups are exposed and should, therefore, be easily accessed for functionalisation.

Post-exfoliation functionalisation of MONs *via* click chemistry

In order to demonstrate the versatility of our click chemistry approach, four different functional groups were introduced using a generalised method: a carboxylic acid, a tertiary amine, an alcohol, and a fluorescent pyrene group. These groups possess a variety of different chemistries, but are also difficult to introduce pre-synthetically, due to both their size and their likelihood to interfere with the formation of the secondary building unit. Cu(N_3-BDC) nanosheets suspended in acetonitrile, were treated with a Cu(I) catalyst, $Cu(CH_3CN)_4PF_6$, and an alkyne-tagged functional group, then stirred at 60 °C for 24 hours. Extensive washings were carried out with THF and diethyl ether to remove excess catalyst and reagent.

Degrees of conversion of ≥80% were obtained for the carboxylic acid (91%), tertiary amine (82%), and alcohol groups (91%), and ~50% for the pyrene group, as determined by ^{1}H NMR spectroscopy of the digested nanosheets (Fig. S20–23†). The reduced degree of functionalisation using the pyrene group is attributed to the significant steric bulk and cone

angle of the pyrene moiety inhibiting reactions at adjacent azide sites. FT-IR spectroscopy further confirms the extent of functionalisation, with a significant reduction in the intensity of the asymmetric (N=N=N) stretch at 2100 cm^{-1} observed for each system, shown in Fig. S21.† Furthermore, the emergence of broad peaks centred around 1050 and 730 cm^{-1} are consistent with previous reports, and are assigned to the introduced triazole group.[30,36–38]

Powder X-ray diffractometry studies show significant peak broadening and reductions in peak intensity for the clicked nanosheets compared to the bulk framework (Fig. S25†). This is an expected consequence of the nanoscopic dimensions of the nanosheets and their lack of three-dimensional extended crystallinity and has been observed by many other authors investigating such nanomaterials.[39–42] However, the peaks that can be identified still align with those of the as-synthesised layered framework or azido-nanosheets, particularly the most intense peak at ~8.6°, indicating that the supramolecular coordination structure was maintained.

The functionalised nanosheets were resuspended in acetonitrile by sonication for 30 seconds and the resulting suspensions exhibit strong Tyndall scattering (Fig. S26†). AFM imaging of these suspensions confirmed that the nanosheet morphology was maintained post-functionalisation. As shown in Fig. 3 (further imaging in S27–30†), the functionalised nanosheets maintain their few-layer thickness across each system. Thicknesses range between 1.8–8.0 nm, with a much narrower distribution than observed for the Cu(N_3-BDC)(DMF) nanosheets (Fig. S31–34†), indicating that the click reaction may have further exfoliated the material. The surface roughness of the –OH and $-CO_2H$ nanosheets are similar to that of the azido-nanosheets, whereas an increase in average roughness is observed for the $-NMe_2$ and –pyr systems. Furthermore, there appears to be no decrease in the lateral size of the nanosheets, attributed to the mild nature of the functionalisation method.

The change in surface properties upon functionalisation was investigated using contact angle goniometry. Equal amounts of each nanosheet system were drop-cast onto identical hot mica plates to form a film, after which the contact angle with a drop of water was investigated. As represented in Fig. 3, there is a clear correlation between the contact angle of the droplet and the hydrophilicity/hydrophobicity or polarity of the group introduced during functionalisation. The acid functionalised nanosheets resulting in an almost completely flat droplet giving a small contact angle, and the pyrene functionalised nanosheets resulting in a significantly more spherical droplet and a larger contact angle.

This procedure of post-exfoliation functionalisation offers several advantages for the patterning of MON surfaces. The versatility of click chemistry means that a range of reactive functional groups (such as acids and amines) can be introduced, and at different ratios. The method uses mild conditions and reagents, meaning this could be extended to other MON systems which have pendant amino functionalities, such as NH_2-MIL-53(Al) nanosheets[43] and Zr_6 systems with ditopic[44] or tritopic[15] linkers as well as amino-functionalised ZIF-7(III) systems.[45]

Furthermore, the lack of pore size constraints in the context of using nanosheets means larger groups, such as polyaromatics or polymers, can be more easily introduced than is often the case for 3D MOFs or unexfoliated layered MOFs.

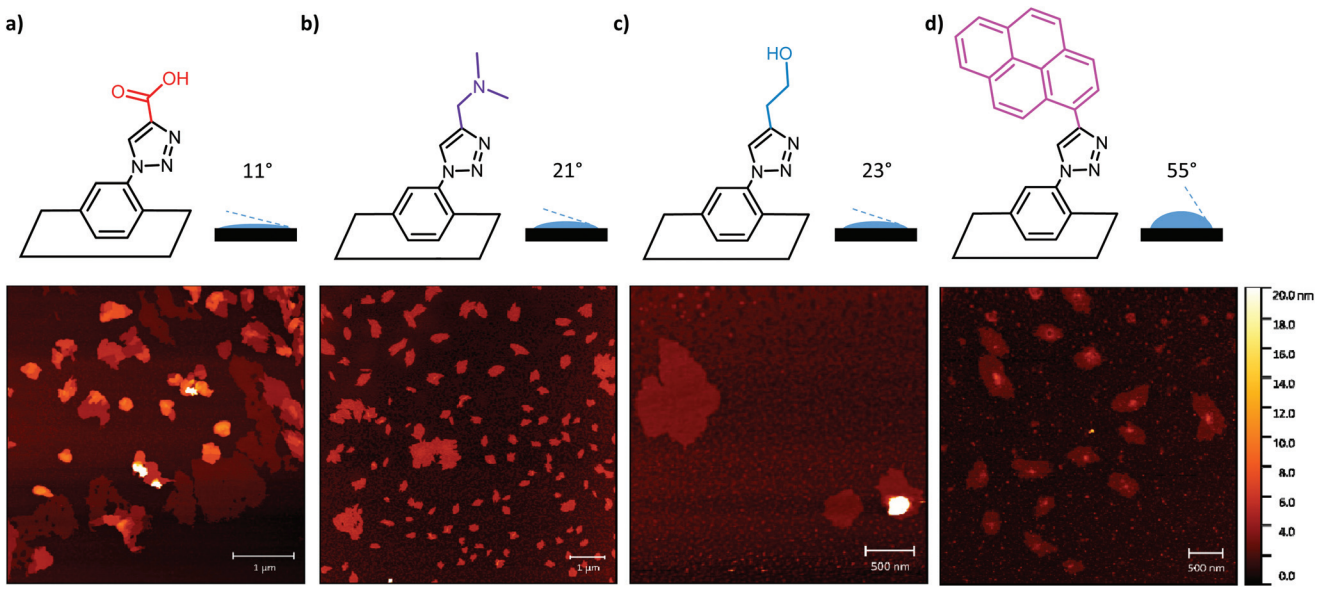

Fig. 3 Structural representations, contact angles with water, and AFM topographical images of the obtained (a) Cu(BDC-trz-CO_2H), (b) Cu(BDC-trz-NMe_2), (c) Cu(BDC-trz-OH), and (d) Cu(BDC-trz-pyr) nanosheets. The water droplet contact angles show a clear trend based on the relative hydrophilicity or polarity of the functional groups introduced.

Sensing experiments

The click-functionalisation of the azido-nanosheets with 1-ethynylpyrene afforded a fluorescent system with high surface area. As pyrene-based MOFs have been frequently targeted for use as sensors,[44] we sought to utilise these electron rich nanosheets for use as sensors in the detection of electron deficient nitrobenzene.

The unfunctionalized azido-nanosheets exhibit absorption maxima at 261 and 332 nm, though neither of these produce an emission upon excitation, thus the unfunctionalized nanosheets are non-fluorescent. Upon ~50% functionalisation with 1-ethynylpyrene, three new absorption maxima appear, at 244, 280 and 351 nm, corresponding to the introduced pyrene group (Fig. S35†). This fluorescence can be observed by the naked eye by application of a UV lamp to the sample (Fig. 4 inset, Fig. S36†). Each of these maxima produce a broad emission spectrum with maxima at 389 and 410 nm. Excitation at 351 nm produces the most intense emission and was thus used for sensing experiments. No excimer formation was observed, which we attribute to the organised and periodic spatial separation of the pyrene groups on the surface of the nanosheets, which prevent the groups from approaching within ~10 Å to form the complex.

Fluorescence quenching titrations were carried by incremental addition of nitrobenzene to a known concentration of the pyrene-functionalised MONs in acetonitrile. As shown in Fig. 4, at increasing concentrations of nitrobenzene, significant decreases in the emission intensity of the Cu(BDC-trz-pyr) MONs were observed. At concentrations of 100 μM, emission intensity was ~99% quenched. This a common mechanism for the sensing of nitroaromatic molecules, a result of charge-transfer between the electrons of photoexcited nanosheets and the LUMO of nitroaromatics, resulting in the quenching of fluorescence.[46] Thus, the electron deficient aromatics introduced here could be extended to the sensing of more energetic and explosive nitroaromatics, such as trinitrotoluene or picric acid.

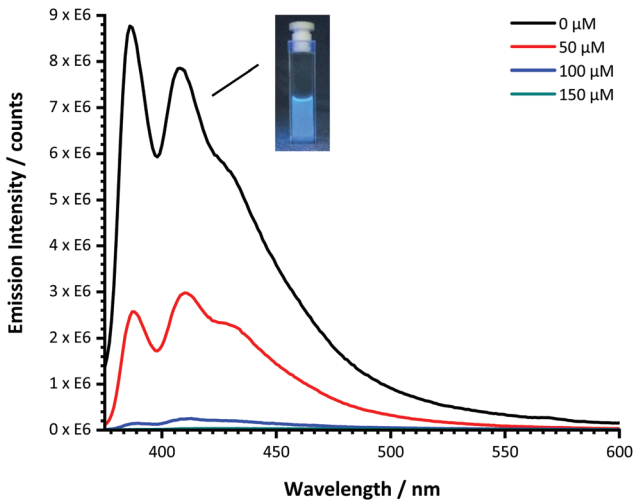

Fig. 4 Emission spectra of Cu(BDC-trz-pyr) MONs in acetonitrile with increasing concentrations of nitrobenzene (λ_{ex} = 351 nm). Inset shows an image of the suspension under a UV lamp.

Conclusion

We demonstrate a new approach to covalently modifying the surface properties of MONs through post-exfoliation functionalisation using convenient and versatile click-chemistry. In the first step, a layered amino-MOF was converted post-synthetically into its azido-form, which was then exfoliated using a mild ultrasonication process to produce few-layer nanosheets. The MONs produced were thinner than those of the parent MOF, attributed to increased inter-layer distance and improved solvent–MON interactions. In the second step, the exposed azide functional groups of the exfoliated nanosheets were functionalised in high yields by reaction with a series of different alkynes. The structure and morphology of the nanosheets remained largely unchanged but contact angle measurements showed their surface chemistry changed to match the polarity of the functional groups added. As a proof of concept, we introduced a photoactive pyrene moiety to the surface of these ultrathin nanosheets and used them for the sensing of nitrobenzene in solution by efficient quenching of the pyrene's fluorescence.

This technique of post-exfoliation functionalisation using click chemistry represents a versatile, robust method for the modification of the surfaces of MONs and other two-dimensional materials. We anticipate that the straightforward addition of new chemical groups using this approach will allow for fine-tuning of the surface properties and functionalities of molecular nanosheets to enable a range of sensing, catalysis, electronics and separation applications.

Experimental

Materials and analytical methods

Materials and reagents were obtained from multiple different commercial suppliers and used without further purification. Chemical sources and all analytical methods are described in S1 of the ESI.†

Post-synthetic functionalisation of Cu(NH_2-BDC)(DMF)

Cu(NH_2-BDC)(DMF) was first prepared according to our previously reported method.[29] The layered amino-MOF (50 mg) was then suspended in THF (5 mL) in a 12 mL reaction vial, then treated with *t*-butyl nitrite (*t*-BuONO) and azidotrimethylsilane (TMS-N_3) in varying equivalents, as outlined in Table S1.† The reaction mixture was gently stirred overnight, with the product MOF obtained by centrifugation (4500 rpm, 10 min). The product was washed with DMF (5 × 10 mL) and diethyl ether (4 × 10 mL), before being left to dry in air, affording Cu(NH_2-BDC)$_x$(N_3-BDC)$_y$(DMF) with varying $x:y$ ratios.

Liquid exfoliation

Cu(N_3-BDC)(DMF) (5 mg) was suspended in acetonitrile (6 mL) in reaction vials with Teflon-lined caps. Samples were sonicated at 80 kHz for 12 hours at 100% power, at a temperature <19 °C and with stirring of the vials to prevent hot-spots. Sonication was followed by centrifugation for 1 hour at 362*g* (1500 rpm) to remove unexfoliated material, followed by separation of the supernatant to obtain a green suspension of Cu (N_3-BDC) MONs.

Post-exfoliation functionalisation of Cu(N_3-BDC) nanosheets

Freshly exfoliated Cu(N_3-BDC) nanosheets in acetonitrile (0.5 mg mL^{-1}, 5 mL) were treated with $Cu(CH_3CN)_4PF_6$ (40 mmol) and acetylene derivatives in varying equivalents, as described in Table S3.† Samples were then heated to 60 °C for 24 hours under a N_2 atmosphere, followed by washes with THF (5 × 10 mL) and diethyl ether (2 × 10 mL), before being left to dry in air, affording click-functionalised nanosheets.

Sensing of nitrobenzene

The fluorescent MONs prepared by the method above were used for sensing studies. A colloidal suspension of Cu(BDC-trz-pyr) nanosheets in acetonitrile (5 mg mL^{-1}) was treated with incremental amounts of nitrobenzene, with emission spectra recorded upon each addition (λ_{ex} = 351 nm). Uniform suspension was assured through use of a vortex mixer before each acquisition.

Conflicts of interest

There are no conflicts to declare.

Acknowledgements

The authors would like to thank the EPSRC (EP/S021124/1) for funding and Michael Harris, Chris Hill and the University of Sheffield BioMedical Sciences EM unit for SEM analysis.

References

1 J. N. Coleman, M. Lotya, A. O. Neill, S. D. Bergin, P. J. King, U. Khan, K. Young, A. Gaucher, S. De, R. J. Smith, I. V. Shvets, S. K. Arora, G. Stanton, H. Kim, K. Lee, G. T. Kim, G. S. Duesberg, T. Hallam, J. J. Boland, J. J. Wang, J. F. Donegan, J. C. Grunlan, G. Moriarty, A. Shmeliov, R. J. Nicholls, J. M. Perkins, E. M. Grieveson, K. Theuwissen, D. W. Mccomb, P. D. Nellist and V. Nicolosi, *Science*, 2011, **331**, 568–572.
2 J. N. Coleman, *Acc. Chem. Res.*, 2013, **46**, 14–22.
3 L. H. Li and Y. Chen, *Adv. Funct. Mater.*, 2016, **26**, 2594–2608.
4 S. Manzeli, D. Ovchinnikov, D. Pasquier, O. V. Yazyev and A. Kis, *Nat. Rev. Mater.*, 2017, **2**, 17033.
5 P. Geng, S. Zheng, H. Tang, R. Zhu, L. Zhang, S. Cao, H. Xue and H. Pang, *Adv. Energy Mater.*, 2018, **8**, 1–26.
6 J. Liu, J. Tang and J. J. Gooding, *J. Mater. Chem.*, 2012, **22**, 12435–12452.
7 L. Daukiya, J. Seibel and S. De Feyter, *Adv. Phys.: X*, 2019, **4**, 1625723.
8 D. Rodríguez-San-Miguel, C. Montoro and F. Zamora, *Chem. Soc. Rev.*, 2020, **49**, 2291–2302.
9 W. Wang, W. Zhao, H. Xu, S. Liu, W. Huang and Q. Zhao, *Coord. Chem. Rev.*, 2020, **429**, 213616.
10 J. Nicks, S. A. Boer, J. A. Foster and N. G. White, *Chem. Sci.*, 2021, **12**, 3322–3327.
11 D. J. Ashworth and J. A. Foster, *J. Mater. Chem. A*, 2018, **6**, 16292–16307.
12 M. Zhao, Y. Huang, Y. Peng, Z. Huang and Q. Ma, *Chem. Soc. Rev.*, 2018, **47**, 6267–6295.
13 Y. Shan, L. Chen, H. Pang and Q. Xu, *Small Struct.*, 2021, **2**, 2000078.
14 J. López-Cabrelles, S. Mañas-Valero, I. J. Vitórica-Yrezábal, P. J. Bereciartua, J. A. Rodríguez-Velamazán, J. C. Waerenborgh, B. J. C. Vieira, D. Davidovikj, P. G. Steeneken, H. S. J. van der Zant, G. Mínguez Espallargas and E. Coronado, *Nat. Chem.*, 2018, **10**, 1001–1007.
15 H. Yuan, G. Liu, Z. Qiao, N. Li, P. J. S. Buenconsejo, S. Xi, A. Karmakar, M. Li, H. Cai, S. J. Pennycook and D. Zhao, *Adv. Mater.*, 2021, **33**, 2101257.
16 C. Tan, K. Yang, J. Dong, Y. Liu, Y. Liu, J. Jiang and Y. Cui, *J. Am. Chem. Soc.*, 2019, **141**, 17685–17695.
17 J. Nicks, K. Sasitharan, R. R. R. Prasad, D. J. Ashworth and J. A. Foster, *Adv. Funct. Mater.*, 2021, **31**, 2103723.
18 S. M. Cohen, *Chem. Rev.*, 2012, **112**, 970–1000.
19 M. Kalaj and S. M. Cohen, *ACS Cent. Sci.*, 2020, **6**, 1046–1057.
20 X. Ling, D. Gong, W. Shi, Z. Xu, W. Han, G. Lan, Y. Li, W. Qin and W. Lin, *J. Am. Chem. Soc.*, 2021, **143**, 1284–1289.
21 Y. Quan, G. Lan, Y. Fan, W. Shi, E. You and W. Lin, *J. Am. Chem. Soc.*, 2020, **142**, 1746–1751.
22 L. Cao, Z. Lin, F. Peng, W. Wang, R. Huang, C. Wang, J. Yan, J. Liang, Z. Zhang, T. Zhang, L. Long, J. Sun and W. Lin, *Angew. Chem., Int. Ed.*, 2016, **55**, 4962–4966.
23 G. Lan, Z. Li, S. S. Veroneau, Y.-Y. Zhu, Z. Xu, C. Wang and W. Lin, *J. Am. Chem. Soc.*, 2018, **140**(39), 12369–12373.
24 J. A. Foster, S. Henke, A. Schneemann, R. A. Fischer and A. K. Cheetham, *Chem. Commun.*, 2016, **52**, 10474–10477.
25 D. J. Ashworth, T. M. Roseveare, A. Schneemann, M. Flint, I. Dominguez Bernáldes, P. Vervoorts, R. A. Fischer, L. Brammer and J. A. Foster, *Inorg. Chem.*, 2019, **58**, 10837–10845.
26 K. Sasitharan, D. G. Bossanyi, N. Vaenas, A. J. Parnell, J. Clark, A. Iraqi, D. G. Lidzey and J. A. Foster, *J. Mater. Chem. A*, 2020, **8**, 6067–6075.
27 J. Nicks, J. Zhang and J. A. Foster, *Chem. Commun.*, 2019, **55**, 8788–8791.

28 J. E. Moses, A. D. Moorhouse, J. E. Moses and K. B. Sharpless, *Chem. Soc. Rev.*, 2007, **8**, 1249–1262.
29 J. Nicks, J. Zhang and J. A. Foster, *Chem. Commun.*, 2019, **55**, 8788–8791.
30 M. Savonnet, E. Kockrick, A. Camarata, D. Bazer-Bachi, N. Bats, V. Lecocq, C. Pinel and D. Farrusseng, *New J. Chem.*, 2011, **35**, 1892.
31 M. Savonnet, D. Bazer-bachi, N. Bats, E. Jeanneau, V. Lecocq, C. Pinel and D. Farrusseng, *J. Am. Chem. Soc.*, 2010, **68**, 4518–4519.
32 X. Zhang, T. Xia, K. Jiang, Y. Cui, Y. Yang and G. Qian, *J. Solid State Chem.*, 2017, **253**, 277–281.
33 M. Savonnet, E. Kockrick, N. Bats, V. Lecocq, C. Pinel and D. Farrusseng, *New J. Chem.*, 2011, **35**, 1892–1897.
34 M. Lotya, A. Rakovich, J. F. Donegan and J. N. Coleman, *Nanotechnology*, 2013, **24**, 265703.
35 D. J. Ashworth, A. Cooper, M. Trueman, R. W. M. Al-Saedi, S. D. Liam, A. J. Meijer and J. A. Foster, *Chem. – Eur. J.*, 2018, **24**, 17986–17996.
36 M. Savonnet, D. Bazer-Bachi, N. Bats, J. Perez-Pellitero, E. Jeanneau, V. Lecocq, C. Pinel and D. Farrusseng, *J. Am. Chem. Soc.*, 2010, **132**, 4518–4519.
37 E. Borello, A. Zechina and E. Guglielminotti, *J. Chem. Soc.*, 1969, 307–311.
38 Y. Tanaka, S. R. Velen and S. I. Miller, *Tetrahedron*, 1973, **29**, 3271–3283.
39 C. F. Holder and R. E. Schaak, *ACS Nano*, 2019, **13**, 7359–7365.
40 S. Gutiérrez-Tarriño, J. L. Olloqui-Sariego, J. J. Calvente, G. M. Espallargas, F. Rey, A. Corma and P. Oña-Burgos, *J. Am. Chem. Soc.*, 2020, **142**, 19198–19208.
41 Y. Liu, L. Liu, X. Chen, Y. Liu, Y. Han and Y. Cui, *J. Am. Chem. Soc.*, 2021, **143**, 3509–3518.
42 G. Ding, Y. Wang, G. Zhang, K. Zhou, K. Zeng, Z. Li, Y. Zhou, C. Zhang, X. Chen and S. T. Han, *Adv. Funct. Mater.*, 2019, **29**, 1–11.
43 Z. Li, D. Zhan, A. Saeed, N. Zhao, J. Wang, W. Xu and J. Liu, *Dalton Trans.*, 2021, **2**, 8540–8548.
44 C. He, K. Lu, D. Liu and W. Lin, *J. Am. Chem. Soc.*, 2014, **136**, 5181–5184.
45 J. López-Cabrelles, S. Mañas-Valero, I. J. Vitórica-Yrezábal, P. J. Bereciartua, J. A. Rodríguez-Velamazán, J. C. Waerenborgh, B. J. C. Vieira, D. Davidovikj, P. G. Steeneken, H. S. J. van der Zant, G. Mínguez Espallargas and E. Coronado, *Nat. Chem.*, 2018, **10**, 1001–1007.
46 F. P. Kinik, A. Ortega-Guerrero, D. Ongari, C. P. Ireland and B. Smit, *Chem. Soc. Rev.*, 2021, **50**, 3143–3177.